

Figure 1: Observational probability of a particular IMF  $B_z$  value (a), and declination of IMF from the ecliptic (b).

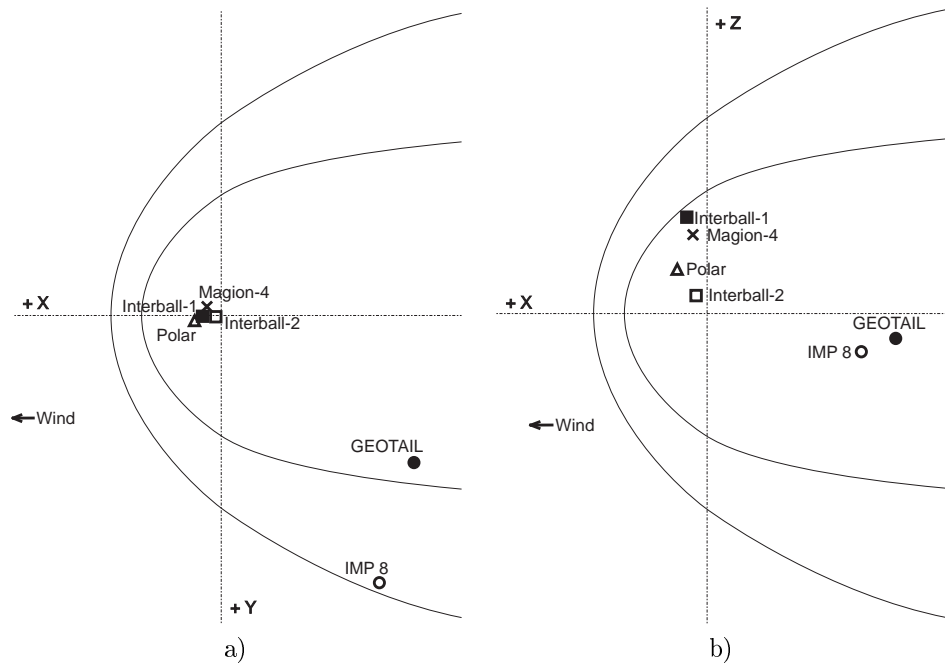


Figure 2: Locations of satellites in GSM co-ordinates.

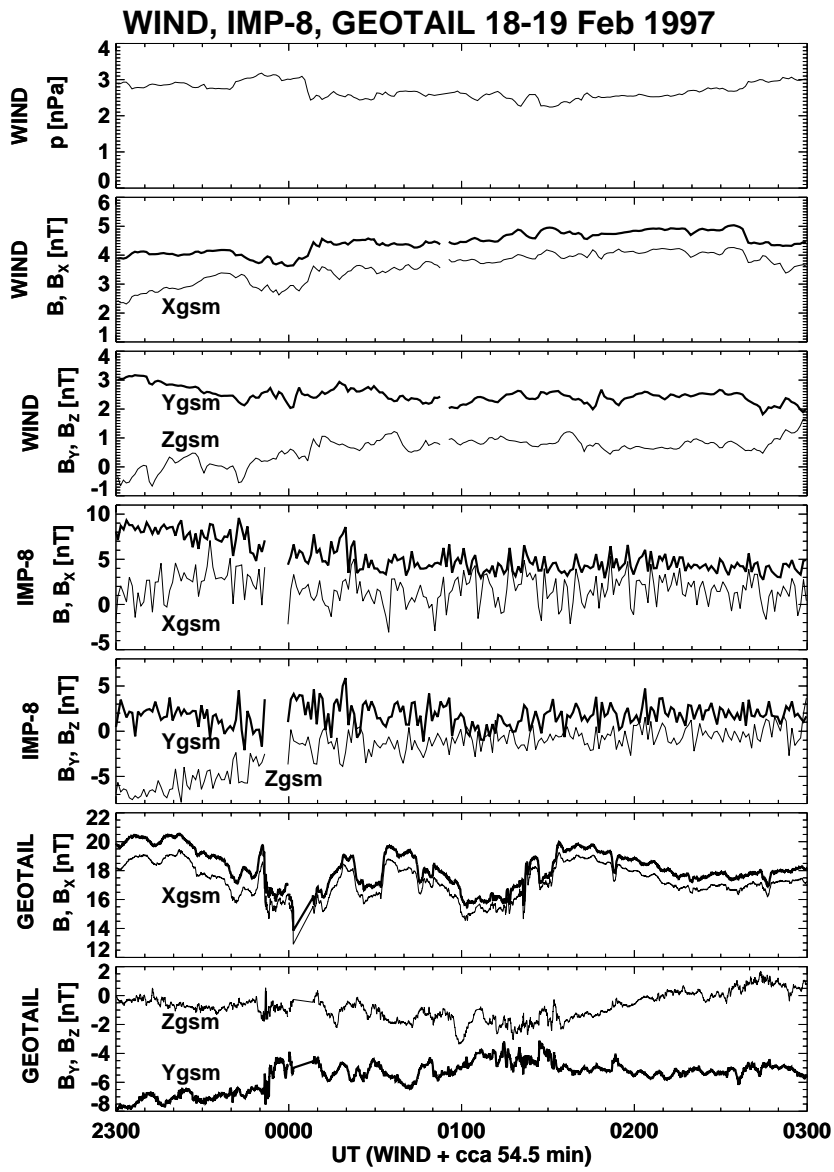


Figure 3: Solar wind and IMF conditions during analyzed interval. From top to bottom: solar wind dynamic pressure; the IMF magnitude and  $B_X$  component; IMF  $B_Y$  and  $B_Z$  components; the magnetosheath magnetic field magnitude and  $B_X$  component; magnetosheath  $B_Y$  and  $B_Z$ ; the plasma sheet magnetic field magnitude and  $B_X$  component;  $B_Y$  and  $B_Z$  components in the plasma sheet. The subscripts in names of panels denote the particular spacecraft. Note that the WIND data are shifted on estimated propagation time.

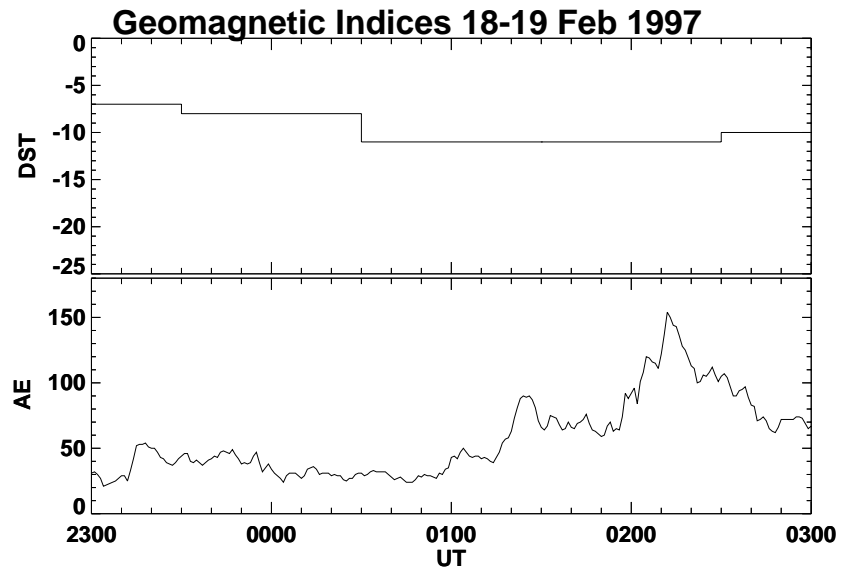


Figure 4: Geomagnetic indexes,  $AE$  and  $D_{ST}$  during the analyzed interval.

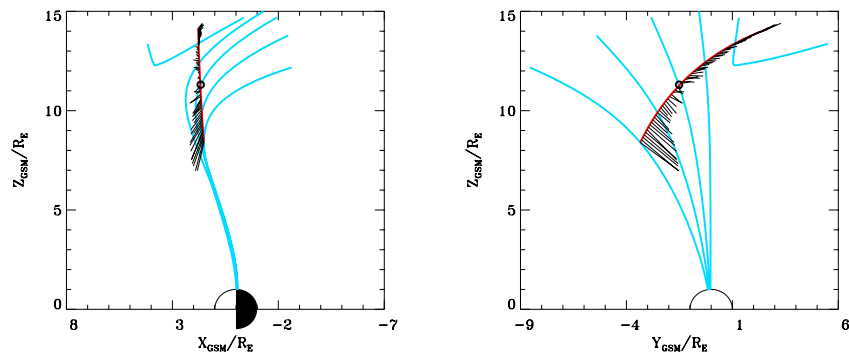


Figure 5: Field lines of the Tsyganenko 96 model (blue) and INTERBALL-1 trajectory (red). INTERBALL-1 moves downward and upward. The black circle denotes the magnetopause crossing. Thin short black abscissae show the measured magnetic field.

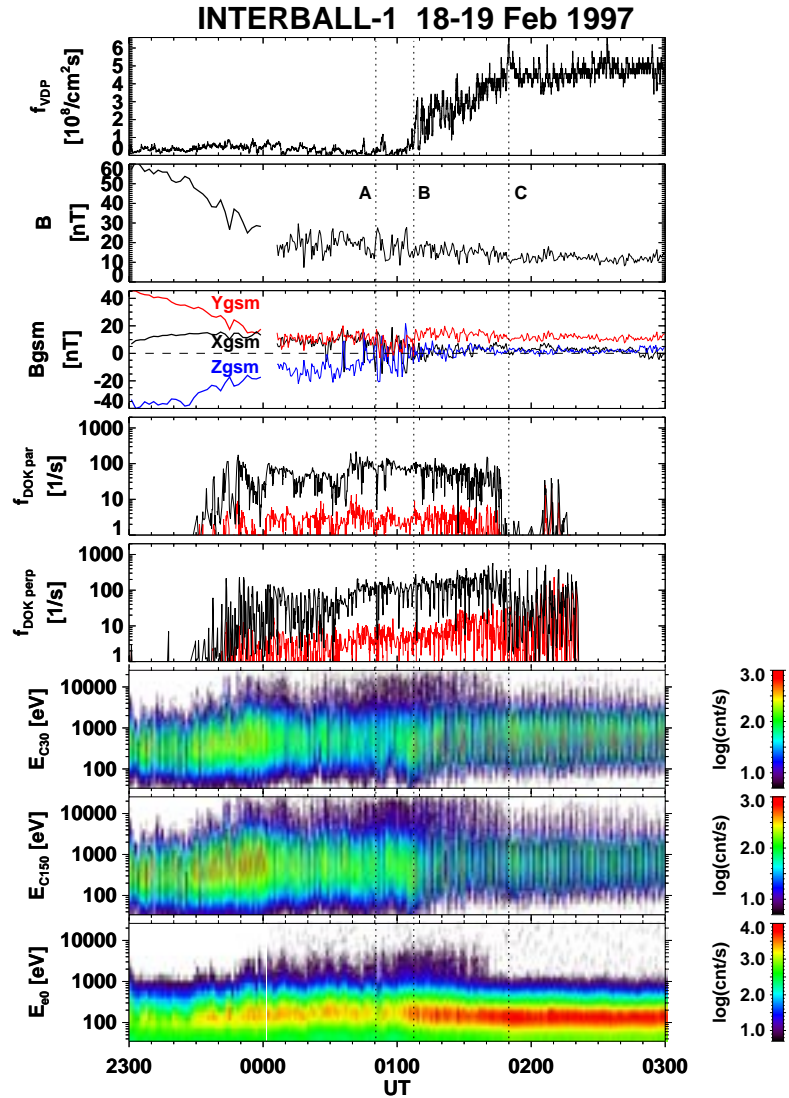


Figure 6: An overview of INTERBALL-1 measurements. From top to bottom:  $f_{VDP}$  - tailward ion flux;  $B$  - magnetic field magnitude;  $B_{gsm}$  - components of the magnetic field;  $f_{DOK_{par}}$  - flux of 51 keV (red) and 111 keV (blue) protons in the sunward direction;  $f_{DOK_{perp}}$  - the same fluxes measured perpendicularly to the s/c spin axis;  $E_{C30}$  and  $E_{C150}$  - ion energy spectrograms measured in sunward and tailward directions, respectively;  $E_{e0}$  - electron energy spectrogram. Vertical lines divide the encountered regions.

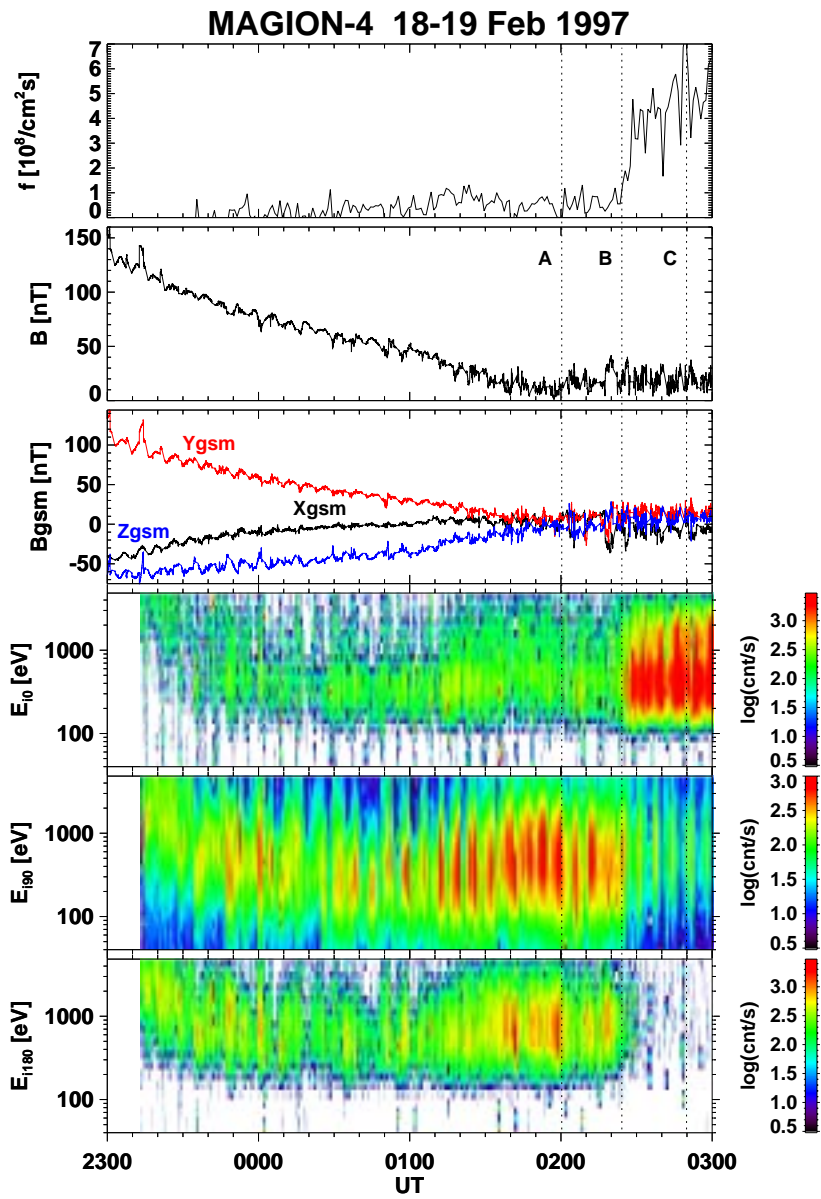


Figure 7: An overview of MAGION-4 observations. From top to bottom:  $f$  - tailward ion flux;  $B$  - magnetic field magnitude,  $B_{gsm}$  - components of the magnetic field;  $E_{i0}$ ,  $E_{i90}$ , and  $E_{i180}$  - ion energy spectrograms measured in tailward, perpendicular, and sunward directions, respectively. Note that the spacecraft spins approximately around the Sun-Earth line with a period *sim7* minutes.

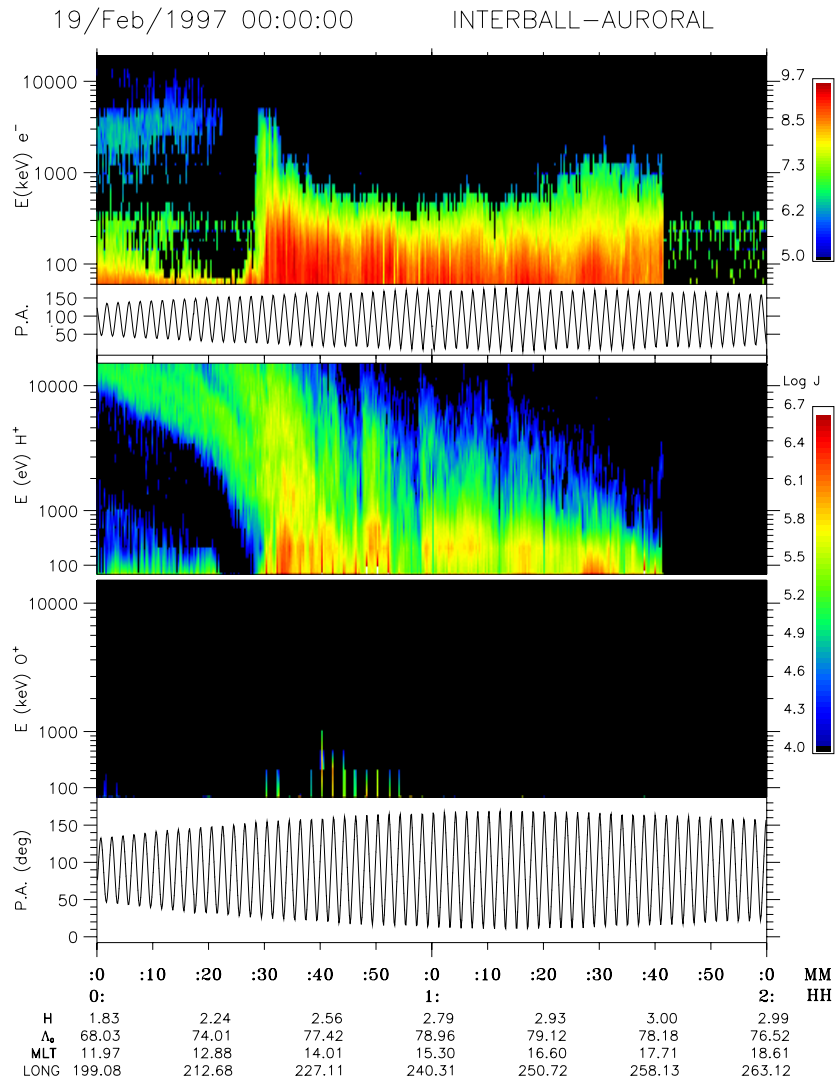
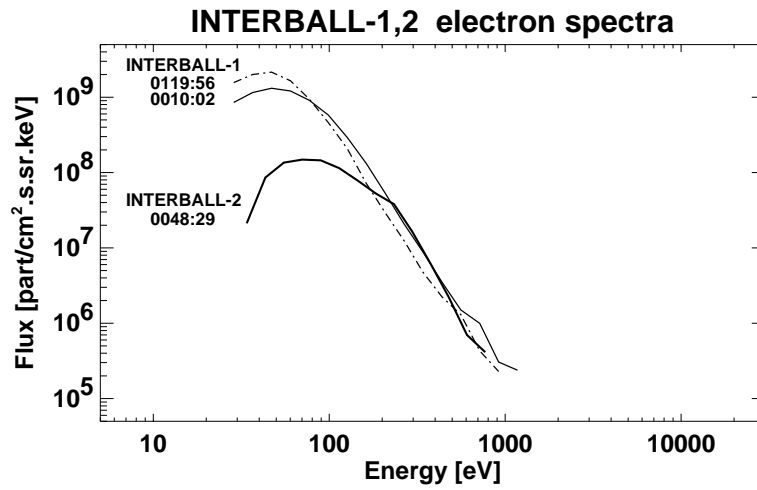
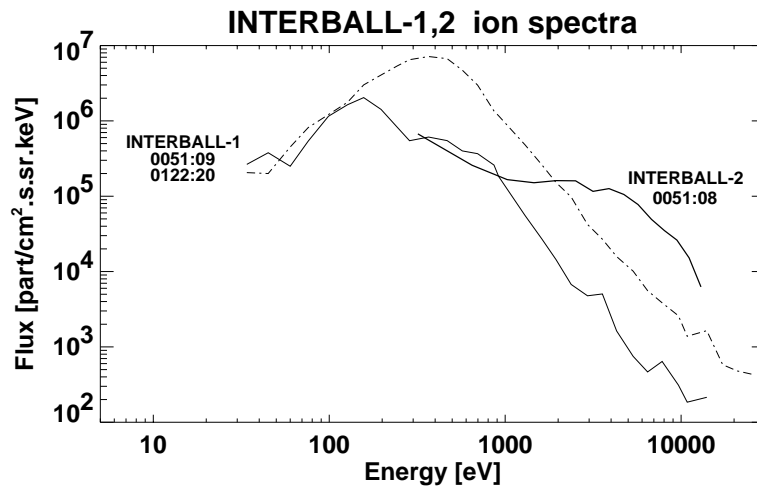


Figure 8: Electron,  $H^+$  and  $O^+$  energy spectrograms in the auroral region as measured by INTERBALL-2. The corresponding pitch angles are shown below.

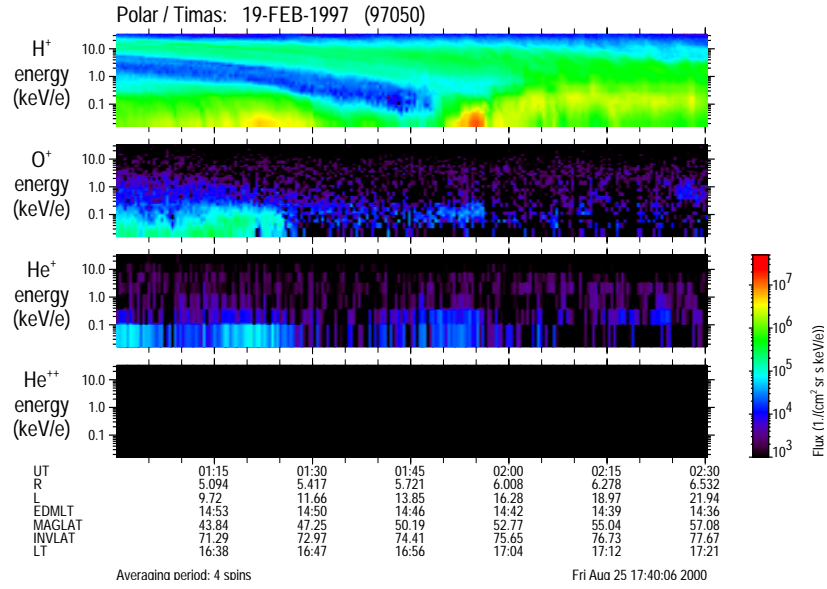


a)

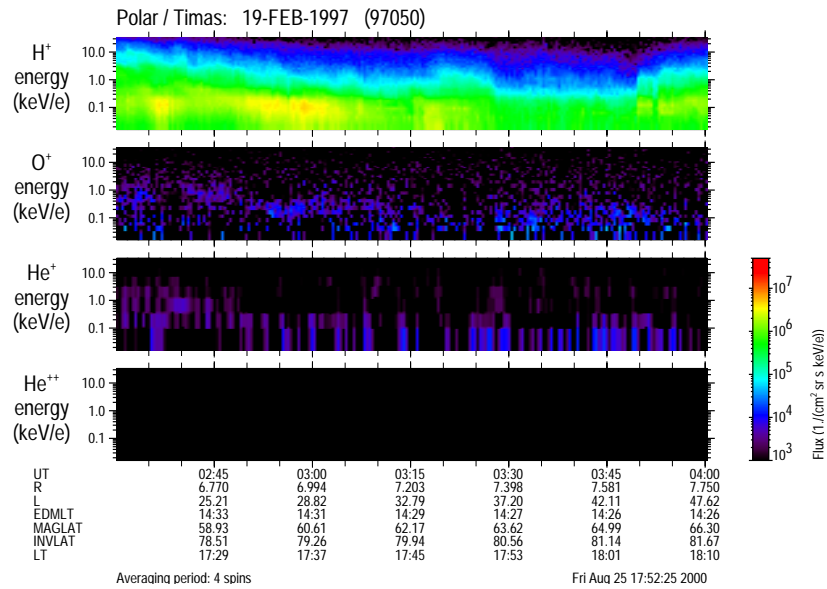


b)

Figure 9: Electron (a) and ion (b) energy spectra as measured by INTERBALL-1 and 2 in the magnetosheath, outer cusp, and LLBL. See text for description.



a)



b)

Figure 10: Polar observations of  $H^+$  and  $O^+$  inside the auroral region.

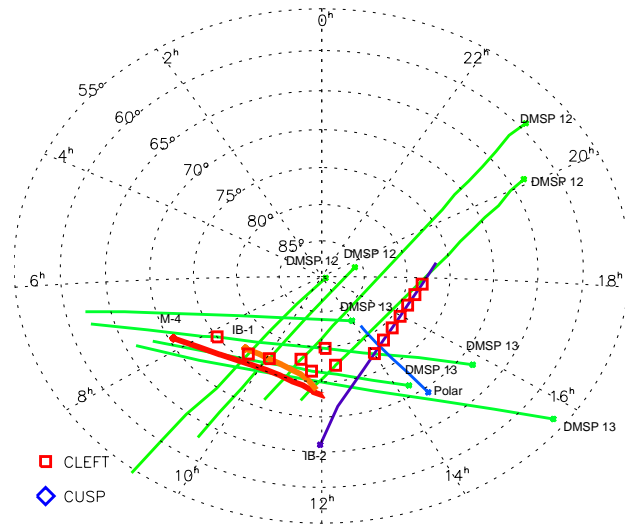


Figure 11: Footprints of the orbit of analyzed satellites (for the northern hemisphere). Depicted time intervals are listed in Table 1. The squares mark the places where cleft plasma was observed. Note that INTERBALL-1 (red) and MAGION-4 (pink) observed the cusp-like plasma along the whole projected part of the orbit.

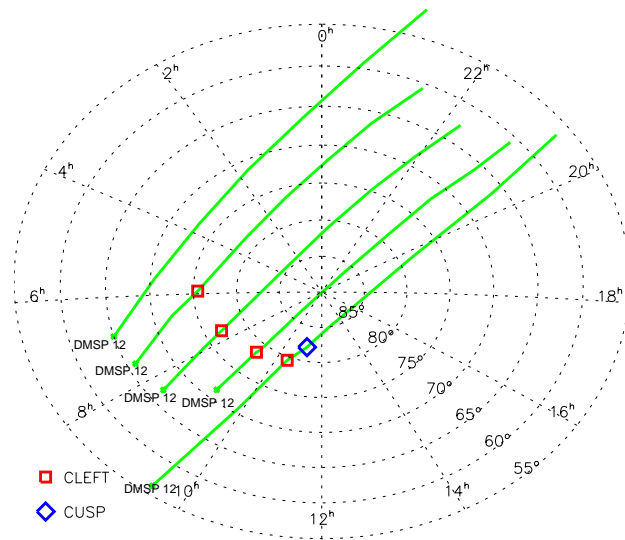


Figure 12: The same as the figure 11, for the southern hemisphere.

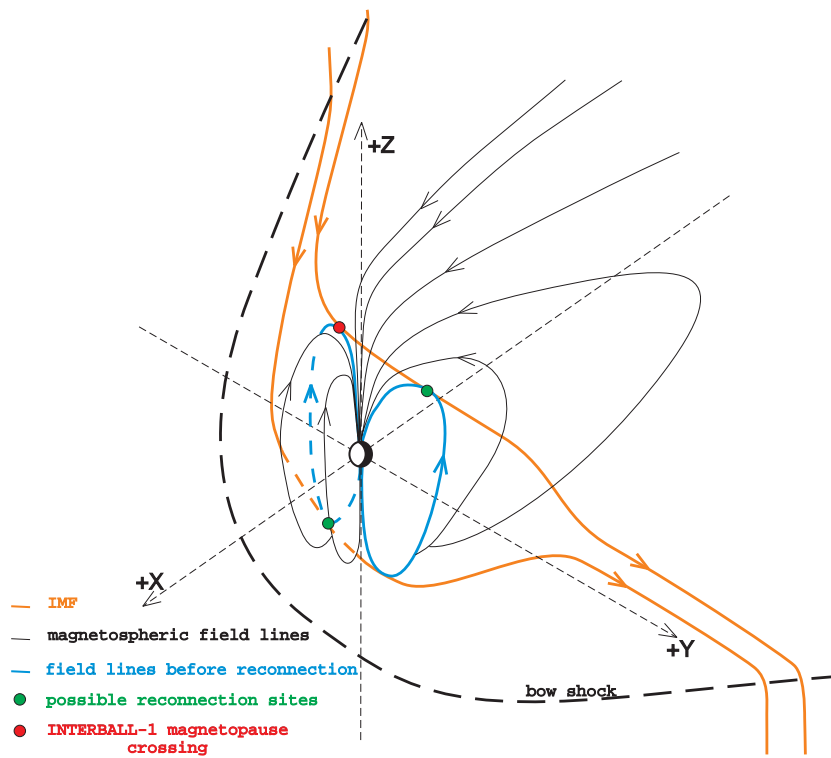


Figure 13: A 3-D sketch of the magnetic field geometry showing possible merging sites when IMF is dominated by the  $B_Y$  component.

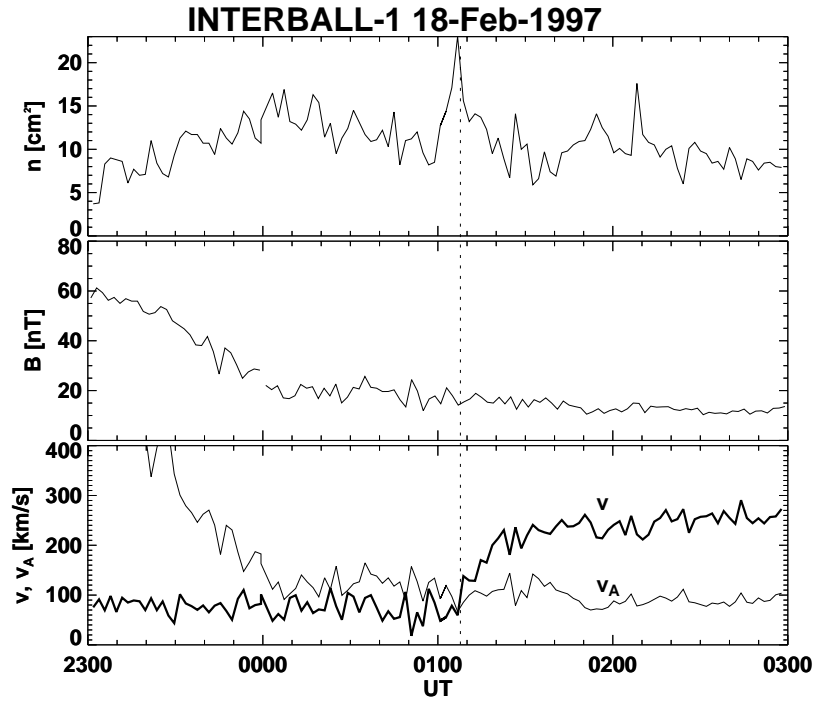


Figure 14: Changes of plasma parameters during the magnetopause crossing as derived from CORALL ion energy spectra (INTERBALL-1). From top to bottom: the ion density,  $n$ ; the magnetic field magnitude,  $B$ ; ion bulk speed,  $v$ ; Alfvén velocity,  $v_A$  calculated form measurements above.

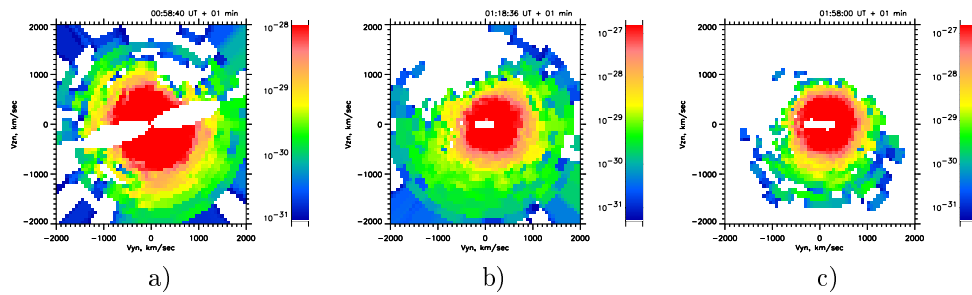


Figure 15: 2-D cuts of 3-D ion velocity distributions as measured in the outer cusp (a), in the reconnection layer (b), and in the magnetoseath (c). The magnetic field points in the  $+Z$  direction,  $+Y$  is the direction of the convection velocity.

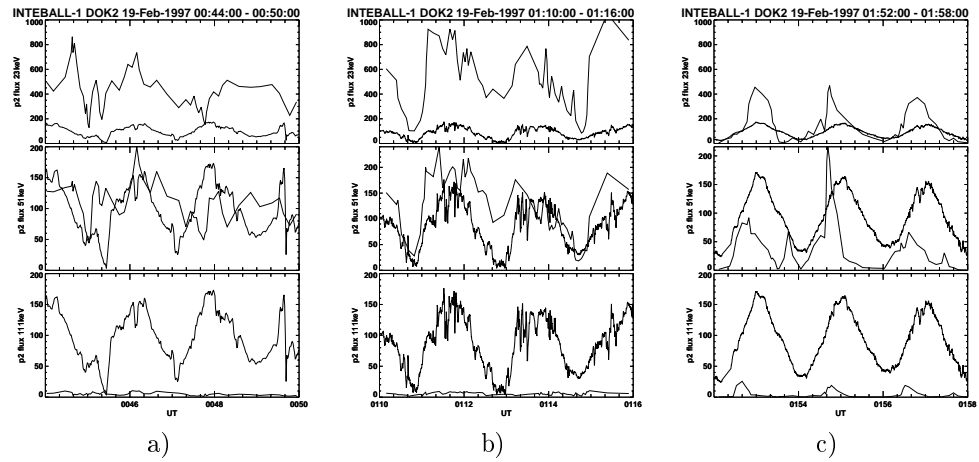


Figure 16: Count rate and corresponding pitch angle measured in the outer cusp (a), reconnection layer (b), and magnetosheath proper (c). The proton energy rises from *sim*23 keV in top panels through 51 keV in middle panels to 111 keV in bottom panels.

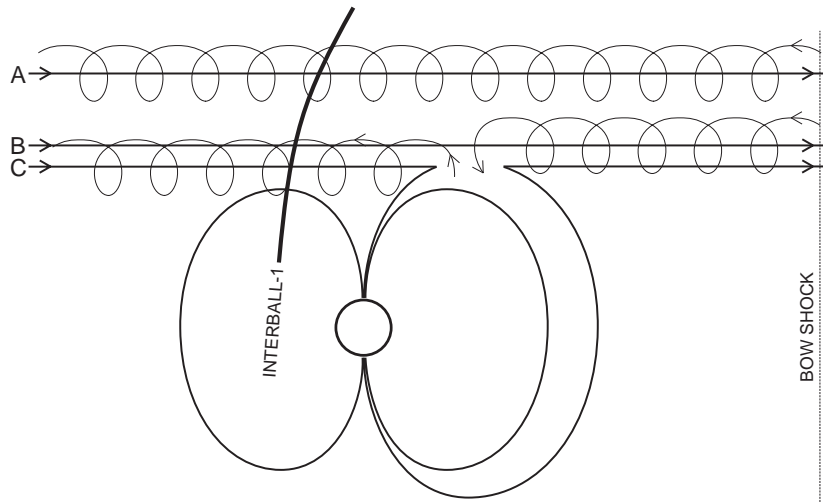


Figure 17: A schematics illustrating the flows of energetic protons. Line A corresponds to the magnetosheath proper, line B represents the magnetosheath field line near the magnetopause and C is the line inside the reconnection layer. Whereas lines A and B are supplied from the bow shock, the source of the particles observed on the line C is the cusp.

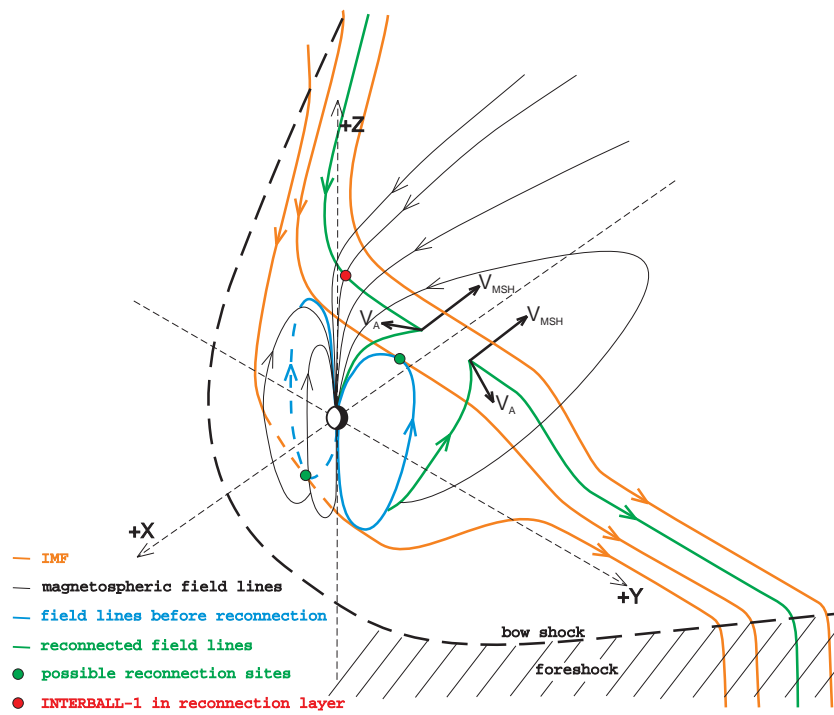


Figure 18: A 3-D sketch of the magnetic field lines formed by reconnection duskward of the northern cusp. The reconnected field line is depicted in green, directions of the motion of the kinks created by reconnection are shown by arrows. See text for a detailed description.